2012 IEEE International Conference on
Multisensor Fusion and Integration for Intelligent Systems (MFI)
September 13-15, 2012. Hamburg, Germany

3-Axis Magnetic Field Mapping and Fusion for Indoor Localization

Etienne Le Grand and Sebastian Thrun, *Stanford University*

Abstract — **As location-based services have grown increasingly popular, they have become limited by the inability to acquire accurate location information in indoor environments, where the Global Positioning System does not function.**

In this field, magnetometers have primarily been used as compasses. As such, they are seen as unreliable sensors when in presence of magnetic field disturbances, which are frequent in indoor environment. This work presents a method to account for and extract useful information from those disturbances. This method leads to improved localization in an indoor environment.

Local magnetic disturbances carry enough information to localize without the help of other sensors. We describe an algorithm allowing to do so as long as we have access to a map of those disturbances. We then expose a fast mapping technique to produce such maps and we apply this technique to show the stability of the magnetic disturbances in time. Finally, the proposed localization algorithm is tested in a realistic situation, showing high-quality localization capability.

I. Introduction

For outdoor localization purposes, magnetometers have been extensively used as compasses to retrieve heading information of a device. The presence of ferromagnetic elements in an indoor environment complicates this task by adding disturbances to the earth's magnetic field. As disturbances there can be much stronger than the natural magnetic field, it becomes impossible to retrieve heading information unless the disturbances are known.

In response to this particularity, methods were developed to detect the presence of disturbances and temporarily remove the magnetometer from the set of sensors used to determine heading determination. One example method is to use and rely on a gyroscope when the magnetometer behaves badly as a compass [1]. This family of methods considers the disturbances as noise which has to be avoided and from which no information can be retrieved.

In this paper, we present an indoor localization system which considers disturbances as a signal rather than as a noise. In fact, the disturbances carry more information than the natural magnetic field. Using only the magnetometer and the accelerometer of a smartphone, our system demonstrates localization capabilities superior to systems using Wi-Fi signal strength maps.

Comparable approaches were exposed in [2] and [3]. The system we describe here differs from the ones described in previous papers by using all three coordinates of the measured magnetic field as an input to the estimation. The additional information gathered frees the system from a dependency on wheel or visual odometry and allows us to relax the assumption of 1-dimensional environments (hallway localization). This requires additional vertical orientation information to be gathered using an accelerometer.

Techniques exploiting local properties of the magnetic field, such as the magnetic field gradient [4], provide useful velocity information. However, they require high frequency magnetometers, and, because they rely only on local properties, also suffer from position drift. As an IMU complement, they can be used in conjunction with the approach presented here.

The system we propose relies on a map of the magnetic field of the building in which we aim to localize. Because such a map is expensive to obtain, we describe a fast 2D mapping procedure. This procedure, similarly to the localization system, requires no more equipment than a smartphone.

II. Magnetometer Sensor Model

The expression of a vector $\boldsymbol{V}$ in frame F is ${}^{F}\boldsymbol{V}$. Consider the phone frame P and the map frame M. ${}^{M}\boldsymbol{V}$ and ${}^{P}\boldsymbol{V}$ are linked through the relation ${}^{P}\boldsymbol{V} = {}^{P}_{M}R\ {}^{M}\boldsymbol{V}$ where ${}^{P}_{M}R$ is the 3x3 rotation matrix from the map frame to the phone frame.

The magnetometer measures the value of the magnetic field at a position in space relative to the orientation of the phone. This value is a vector of three coordinates, each one representing the value of the magnetic field along one direction of the phone's frame $(x_{phone}, y_{phone}, z_{phone})$:

$$ {}^{P}\boldsymbol{B}^{measured} = \left(B^{measured}_{x_{phone}}, B^{measured}_{y_{phone}}, B^{measured}_{z_{phone}}\right) \quad (1)$$

As the measurement lies in a 3-dimensional space, we can expect to extract more information from it than a simple heading, which lies in a 1 dimensional space.

Phone applications do not usually have access to the raw output of the magnetic sensor. Instead, they receive values resulting from a filtering, often performed on the sensor chip itself. Hence, measurement errors, such as those due to hard iron biases, soft iron biases, scale factor errors, and misalignment errors, are altered by the filtering and cannot be measured and eliminated using common approaches [5].

Because of this restriction, we use a simple sensor model for the magnetometer:

$$ {}^{P}\boldsymbol{B}^{measured} = {}^{P}\boldsymbol{B}^{real} + {}^{P}\boldsymbol{B}^{offset} + {}^{P}\boldsymbol{B}^{sensor\_noise} \quad (2)$$

where the first term corresponds to the magnetic field the magnetometer would measure if it was perfect and calibrated.

$$ {}^{P}B^{real} = {}^{P}_{M}R\,{}^{M}B^{real} \tag{3} $$

$\boldsymbol{B}^{offset}$ is the offset of the magnetometer, which slowly drifts over time. $\boldsymbol{B}^{offset}$ only has a meaning in the phone frame and does not depend on the orientation of the phone. Varying the orientation of the phone without changing its position allows us to calculate this offset. In particular, if the phone's position is kept constant, a 180° rotation around the $\boldsymbol{z}_{phone}$ axis leads to

$$ \begin{bmatrix} B_x^{offset} \\ B_y^{offset} \\ 0 \end{bmatrix} = \frac{{}^{P}\boldsymbol{B}^{measured}_{original} + {}^{P}\boldsymbol{B}^{measured}_{rotated}}{2} \tag{4} $$

Similarly, the $\boldsymbol{z}_{phone}$ component of the offset can be determined by a rotation around $\boldsymbol{x}_{phone}$ or $\boldsymbol{y}_{phone}$. In the following, we will suppose that the offset is known and cancelled. The sensor model becomes

$$ {}^{P}\boldsymbol{B}^{measured} = {}^{P}_{M}R\,{}^{M}\boldsymbol{B}^{real}(\boldsymbol{p}) + {}^{P}\boldsymbol{B}^{sensor\_noise} \tag{5} $$

$\boldsymbol{B}^{sensor\_noise}$ is a small term representing the part of sensor noise which cannot be explained by calibration drift. $\boldsymbol{p}$ represents the position of the phone in the map frame. This equation shows that the measured magnetic field and the phone's position $\boldsymbol{p}$ and orientation ${}^{P}_{M}R$ are tightly coupled through the knowledge of the magnetic field in the building ${}^{\mathrm{M}}\mathbf{B}^{real}$. This coupling can be effectively used by a Bayes filter to extract position and orientation information from magnetic field measurements. This can be done only if we already have a map of the magnetic field ${}^{\mathrm{M}}\mathbf{B}^{real}$.

Collecting a 3D map of the magnetic field is an expensive operation. For simplicity, we suppose that the phone's altitude p_z is fixed. Hence, we only need a 2D map of the magnetic field. Generalization to 3D maps is possible by interpolation of magnetic field measurements from a 2D envelope of the 3D space as long as this 3D space does not contain ferromagnetic objects.

Changes in the environment affect the magnetic field. As we cannot recollect the map often, we model those map inconsistencies by an isotropic random noise.

$$ {}^{\mathrm{M}}\mathbf{B}^{real} = {}^{\mathrm{M}}\mathbf{B}^{mapped} + {}^{\mathrm{M}}\mathbf{B}^{\mathrm{environment\_noise}} \tag{6} $$

Note that the noise due to environment changes has a much greater amplitude than the sensor noise. The sensor model becomes

$$ {}^{\mathrm{P}}\mathbf{B}^{measured} = {}^{P}_{M}R\,{}^{\mathrm{M}}\mathbf{B}^{mapped}(\boldsymbol{p}) + {}^{P}\boldsymbol{B}^{noise} \tag{7} $$

Bayes' rule hence gives the following formula for the probability of being at a position $\boldsymbol{p}$ and orientation ${}^{P}_{M}R$ given the measured and the mapped magnetic fields:

$$ P\left(\boldsymbol{p}, {}^{P}_{M}R \middle|\, {}^{\mathrm{P}}\mathbf{B}^{measured}\right) \propto P\left({}^{P}\boldsymbol{B}^{noise} = {}^{\mathrm{P}}\mathbf{B}^{measured} - {}^{P}_{M}R\,{}^{\mathrm{M}}\mathbf{B}^{mapped}(\boldsymbol{p})\right) \tag{8} $$

III. Accelerometer Information

The orientation of the phone can be related to the orientation of the user relative to the room if the phone is held in a constant position for a few seconds. In particular, averaging the accelerometer reading, we can determine the expression of the gravity vector in the phone frame. This fixes two degrees of freedom of ${}^{P}_{M}R$. The remaining degree of freedom is a yaw corresponding to the heading of the user θ_{user}.

In the event of a walking user, it is possible to use the accelerometer as a pedometer, to estimate the current step frequency. We decided to present results which were obtained without the use of this estimate in order to emphasize the capability the magnetometer has on its own.

IV. Particle Filter

The localization is performed using a particle filter [6] on a state space of dimension 5:

$$ s = \left(p_x, p_y, \theta_{user}, v_{user}, \omega_{user}\right) = (x, y, \theta, v, \omega) $$

Where x, y, θ represent the user's position and orientation in the room, v is the user's forward velocity and ω is the user's rotational speed. We model the motion by a random linear and angular acceleration terms $\varepsilon^{linear}_{acceleration}$ and $\varepsilon^{angular}_{acceleration}$.

$$ v(t+\Delta t) = v(\mathrm{t}) + \varepsilon^{linear}_{acceleration}\Delta \mathrm{t} \tag{9} $$

$$ \omega(t+\Delta t) = \omega(t) + \varepsilon^{angular}_{acceleration}\Delta \mathrm{t} \tag{10} $$

$$ \begin{bmatrix} x(t+\Delta t) \\ y(t+\Delta t) \end{bmatrix} = \begin{bmatrix} x(t) \\ y(t) \end{bmatrix} + \begin{bmatrix} cos(\theta(t)) \\ sin(\theta(t)) \end{bmatrix} v(t+\Delta t)\Delta t \tag{11} $$

$$ \theta(t+\Delta t) = \theta(t) + \omega(t+\Delta t)\Delta t \tag{12} $$

The sensor update makes indirect use of accelerometer measurements through $R_{\boldsymbol{z}}(\theta)$ and direct use of the magnetometer measurement.

$$ P\left(x, y, z, \theta \middle|\, {}^{\mathrm{P}}\mathbf{B}^{measured}\right) \propto P\left({}^{P}\boldsymbol{B}^{noise} = {}^{\mathrm{P}}\mathbf{B}^{measured} - \mathrm{R}_{\mathbf{z}}(\theta)\,{}^{\mathrm{M}}\mathbf{B}^{mapped}(x, y, z)\right) \tag{13} $$

where

$$ R_{\boldsymbol{z}}(\theta) = \begin{bmatrix} \cos(\theta) & -\sin(\theta) & 0 \\ \sin(\theta) & \cos(\theta) & 0 \\ 0 & 0 & 1 \end{bmatrix} \tag{14} $$

The probability distribution of ${}^{P}\boldsymbol{B}^{noise}$ is hard to characterize as the changes in environment can have small or large impact: big metallic furniture or building structure are the main magnetic field disturbances sources. $P\left({}^{P}\boldsymbol{B}^{noise}\right)$ depends on the frequency at which this kind of changes in the environment occurs and on the age of the map.

We use an isotropic heavy-tailed Gaussian pseudo-distribution that does not sum to 1:

$$ P\left({}^{P}\boldsymbol{B}^{noise}\right) \propto \exp\left(-\frac{1}{2}\frac{\left\|{}^{P}\boldsymbol{B}^{noise}\right\|^2}{\sigma^2}\right) + c, \tag{15} $$

$$ \sigma = 10\mu T, \qquad c = 0.2 $$

V. MAPPING

The sensor update of our particle filter (13) requires a map of the magnetic field of the room. Building such a map is not a common or straightforward task. One way would be to measure the magnetic field at each point of a dense 3D grid of the room. This method would require additional equipment such as a way to localize accurately the magnetometer while it is taking measurements. This could be done by 3D visual tracking or by mounting the magnetometer on a robot which would travel the room while taking measurements. In both cases, mapping even a single room would take a long time.

We present here a fast 2D mapping method using a single smartphone. The 3D case can then be considered as a generalization of the 2D case either by:

- Disposing a higher number of phones/magnetometers and building 2D maps at different heights at the same time, then interpolating values between the planes.
- Or building the magnetic field map on a contour of a free 3D space and using Maxwell's laws to calculate the values of the magnetic field at any point inside this free space.

We build the map of the magnetic field of the plane $z = z_{user}$ manually by covering the room twice in serpentines to form a square grid (Fig. 1). We record the magnetic field along lines parallel to the x axis of the room, then along lines parallel to the y axis.

The beginning and the end of each line is marked by a timestamp to delimit which sequence of measurements corresponds to which line. We control the orientation of the phone when collecting data on each of the lines, so we know this orientation and we can rotate the measured magnetic field and work with its expression in the map frame.

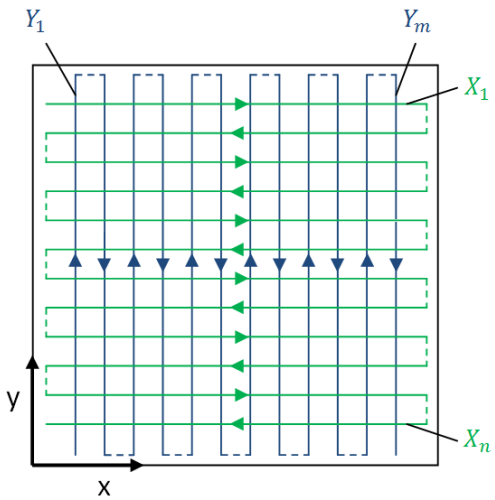

Fig. 1. Path followed to build the magnetic field map, first on lines parallel to $\boldsymbol{x}$, then on lines parallel to $\boldsymbol{y}$.

The data collected can be represented by two sets of three images, each representing one coordinate of the magnetic field as measured during a one-direction mapping. The first set of 3 images is shown in Fig. 2.

If the speed during the data collection was constant along each line and if the sensor's offset was null, the images would already correspond to maps of the magnetic field.

The effect of the bad calibration of the phone is obvious on B_x and B_y: the orientation of the phone relative to the map changed between each line because the phone's orientation was different between consecutive lines. We followed the even-numbered lines left to right and the odd-numbered lines right to left. This causes the x and y components of the offset to be added to the even lines and subtracted to the odd lines, creating the striping effect visible on B_x and B_y. This allows to determine B_x^{offset} and B_y^{offset} by minimizing the discontinuities between consecutive lines. To determine B_z^{offset}, another method must be used, for example simply flipping the phone upside down while keeping its position constant. The resulting images once the offsets are cancelled are shown in Fig. 3.

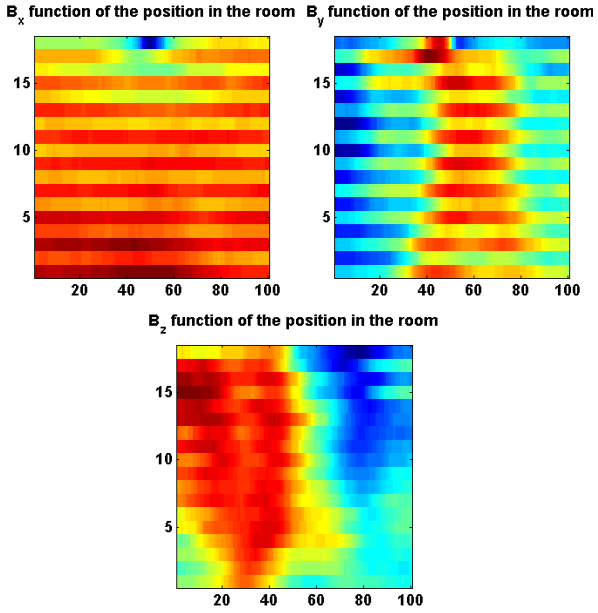

Fig. 2. Magnetic field as measured during the mapping along the lines parallel to $\boldsymbol{x}$. The y axis on the graphic corresponds to the number of the line and the x axis corresponds to the time of the measurement relative to the moments we started and finished following each line. Values are scaled and color-coded independently for each coordinate to better show spatial variations.

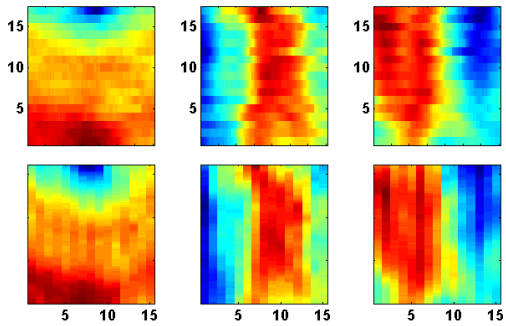

Fig. 3. The 6 images once the offsets on x and y are cancelled. Magnetic field components (x: left, y: middle and z: right) as measured when following the lines parallel to x (top) or y (bottom)

Let $X_1 \dots X_n$ be the lines parallel to $\boldsymbol{x}$ and $Y_1 \dots Y_m$ the lines parallel to $\boldsymbol{y}$. We denote the magnetic field measured on the line $L \in \{X_1, \dots, X_n, Y_1, \dots, Y_m\}$ by ${}^{\mathrm{M}}\mathbf{B}^{measured}_{along\ L}$

In order to build the map, we need to know the position $x_L(t), y_L(t)$ at which the measurement ${}^{\mathrm{P}}\mathbf{B}^{measured}_{along\ L}(\mathrm{t})$ was made. On X_i, $y_{X_i}(t) = y_{X_i}$ is constant by definition, and $x_{X_i}(t)$ has to be estimated. It is smooth and reflects the mapper's instantaneous walking speed. Conversely, while following a line parallel to the y axis, we know $x_{Y_j}(t) = x_{Y_j}$ but we do not know $y_{Y_j}(t)$.

Each Y_i intersects each X_j at one point of the grid. At those locations, the magnetic field measured on both lines should be the same once the offsets have been cancelled. Let $t^j_{X_i}$ and $t^i_{X_j}$ be the times at which $X_i \cap Y_j$ is attained while measuring the magnetic field respectively along the X_i and Y_j lines. We must have

$$ {}^{\mathrm{M}}\mathbf{B}^{measured}_{along\ \mathrm{X_i}}(t^j_{X_i}) \approx {}^{\mathrm{M}}\mathbf{B}^{measured}_{along\ \mathrm{Y_j}}(t^i_{Yj}) \quad (16) $$

Also, if our speed does not change too much while we walk along one line, the time interval between two intersections on one line should be constant:

$$ t^{j+1}_{X_i} - t^j_{X_i} \approx dt_{X_i} = cst,\ t^{i+1}_{Y_j} - t^i_{Y_j} \approx dt_{Y_j} = cst \quad (17) $$

An iterative gradient descent energy minimization algorithm minimizes the sum of violation of this set of constraints

$$ \sum_{i,j} \left\| {}^{\mathrm{M}}\mathbf{B}^{measured}_{along\ \mathrm{X_i}}(t^j_{X_i}) - {}^{\mathrm{M}}\mathbf{B}^{measured}_{\mathrm{along\ Y_j}}(t^i_{Yj}) \right\| \quad (18) $$

The output of this algorithm is an estimate of $t^j_{X_i}, t^i_{Y_j}, i = 1 \dots n, j = 1 \dots m$. The functions $x_{Y_j}(t)$ and $y_{X_i}(t)$ are then interpolated from the known points $x_{X_i}\left(t^j_{X_i}\right) = x_{Y_j}$ and $y_{Y_j}\left(t^i_{Y_j}\right) = y_{X_i}$

We now have a set of positions along $n + m$ lines for which we have measurements.

$$ \forall i \in [\![1, n]\!], x_{X_i}(t), y_{X_i}, {}^{M}\boldsymbol{B}^{measured}_{along\ X_i}(t) \quad (18) $$

$$ \forall j \in [\![1, m]\!], x_{Y_j}, y_{Y_j}(t), {}^{M}\boldsymbol{B}^{measured}_{along\ Y_j}(t) \quad (19) $$

Those positions describe a mesh, on which we have mapped the magnetic field. We populate the rest of the map by linear interpolation from the mesh. A first dense estimate ${}^{M}\boldsymbol{B}^{X}$ of the magnetic field is computed by interpolating only from the measurements along the X lines (18).

If $\alpha \in [0,1]$,

$$ x = x_{X_i}(t_1) = x_{X_{i+1}}(t_2), \text{ and} \quad (20) $$

$$ y = (1-\alpha) y_{X_i} + \alpha y_{X_{i+1}}, \text{ then} $$

$$ {}^{M}\boldsymbol{B}^{X}(x,y) = \quad (21) $$

$$ (1-\alpha)\, {}^{M}\boldsymbol{B}^{measured}_{along\ X_i}(t_1) + \alpha\, {}^{M}\boldsymbol{B}^{measured}_{along\ X_{i+1}}(t_2) $$

Similarly, a second estimate ${}^{M}\boldsymbol{B}^{Y}$ is computed by interpolating only from measurements along the Y lines (19). The two estimates are then averaged:

$$ {}^{M}\boldsymbol{B}^{mapped} = \frac{{}^{M}\boldsymbol{B}^{X} + {}^{M}\boldsymbol{B}^{Y}}{2} \quad (22) $$

Although ${}^{M}\boldsymbol{B}^{mapped}$ is the result of interpolations, it preserves most of the spatial high frequency information present in the magnetic field. Variations of the magnetic field along the x axis were captured when walking along the X_i lines and are encoded into ${}^{M}\boldsymbol{B}^{X}$. High frequency information along the y axis is similarly encoded into ${}^{M}\boldsymbol{B}^{Y}$. By averaging ${}^{M}\boldsymbol{B}^{X}$ and ${}^{M}\boldsymbol{B}^{Y}$, we ensure that ${}^{M}\boldsymbol{B}^{mapped}$ conserves high frequency information along both axis, with at most a loss of 3db in amplitude.

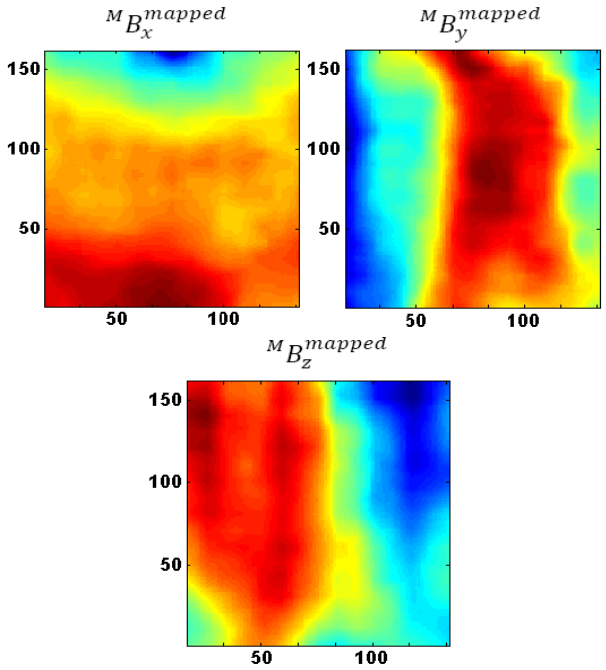

Fig. 4. Magnetic field map resulting from the interpolation of the mesh once the intersections of the lines are found. Marks on the axes are in 10^{th} of the initial unit: the distance separating two collection lines. It is 7cm in this case.

When considering the size of the room as a constant, the time needed to collect the data with this technique is proportional to $(n + m)$ instead of being proportional to $(n * m)$, as for the usual technique of measuring the magnetic field precisely on each point of the grid. Hence, n and m can easily be made big enough, and the grid step small enough, to have only little variations of the magnetic field over the linear interpolation intervals.

As Fig. 4 shows, ${}^{M}\boldsymbol{B}^{mapped}$ variations have lower frequency than the mapping step. This validates our choice of grid step size ensuring that most of the spatial information is preserved during interpolation. Fig. 4 also shows that the magnetic field varies significantly over the mapped area. This finding is crucial as it explains why it is possible to localize using exclusively the magnetometer. The measured magnetic field is highly coupled with the position at which the measurement is taken.

To rely on a map of the magnetic field, we must determine how long such a map is valid. Studying the stability of the magnetic field in time gives us information on ${}^{M}\boldsymbol{B}^{noise}$. We built the map of the same room 4 times with 1 week intervals between each mapping. The first 3 times, the room was empty; the 4^{th} time, 20 students were working here, about 10 of which had laptops. The resulting maps are presented in Fig. 5.

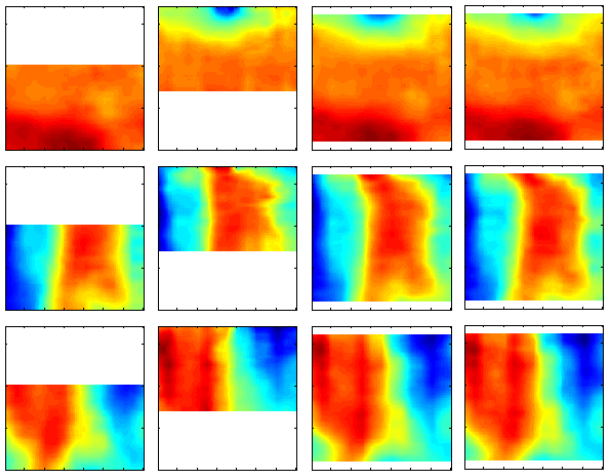

Fig. 5. Magnetic field maps obtained at 1 week intervals. Top: B_x, middle: B_y, bottom: B_z. Each column corresponds to the magnetic field mapped a certain week. Not all of the room was mapped each time. The white areas correspond to non-mapped spaces. The magnetic field does not vary significantly through the weeks nor based on the presence or absence of consumer electronic devices.

The structure of the building did not change between captures, but furniture changed. The maps created at different times are extremely similar, hinting that the distribution of ${}^{M}\boldsymbol{B}^{noise}$ is very narrow around $\mathbf{0}$: the information we can obtain from the magnetic field has a high signal on noise ratio. The presence or absence of people and laptops in the room does not affect significantly the magnetic field either. These characteristics allow for a working magnetometer-based localization system.

VI. Localization Results

To test the particle filter described in section IV with the maps created in section V, we collected magnetometer information while walking along two simple trajectories drawn on the ground: a circle and a line. This choice of trajectories was dictated by our lack of tracking system needed to obtain ground truth in more complex trajectories. The data was then fed into a particle filter running on a laptop.

The particle filter was initialized with ten thousand particles distributed uniformly over the room and over a reasonable walking speed range. When solving the global localization problem, Wi-Fi would typically be used to determine a coarse location to use as prior. The results of the localization are presented in Fig. 6 and 7.

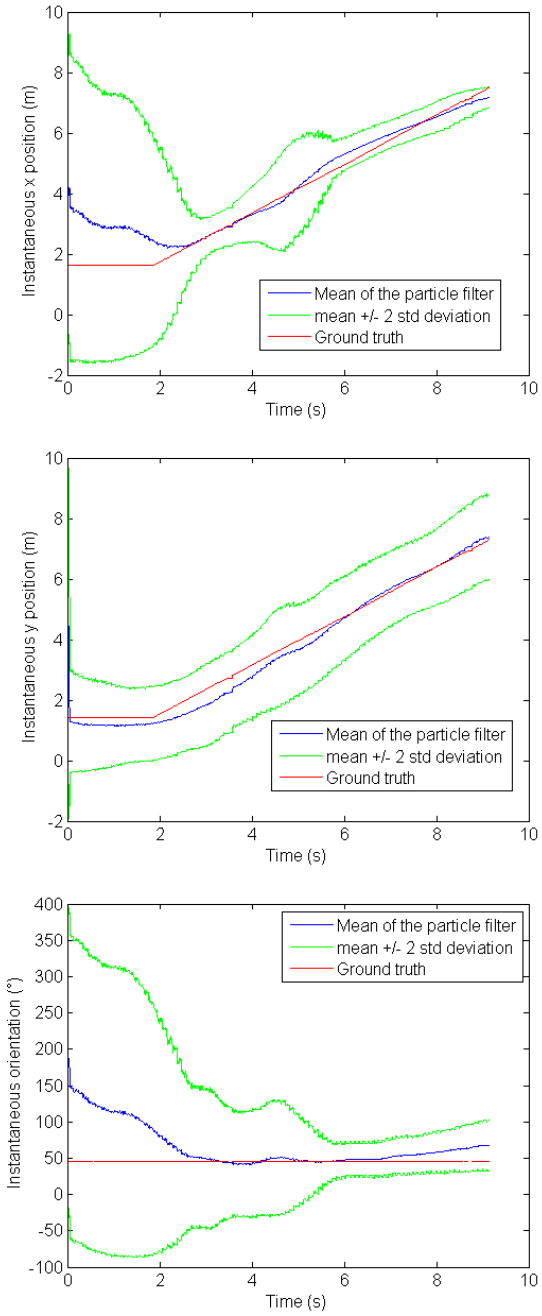

Fig. 6. Comparison of the mean instantaneous position (top: along x, middle: along y) and orientation (bottom) of the particle filter with the ground truth in the case of the straight line trajectory.

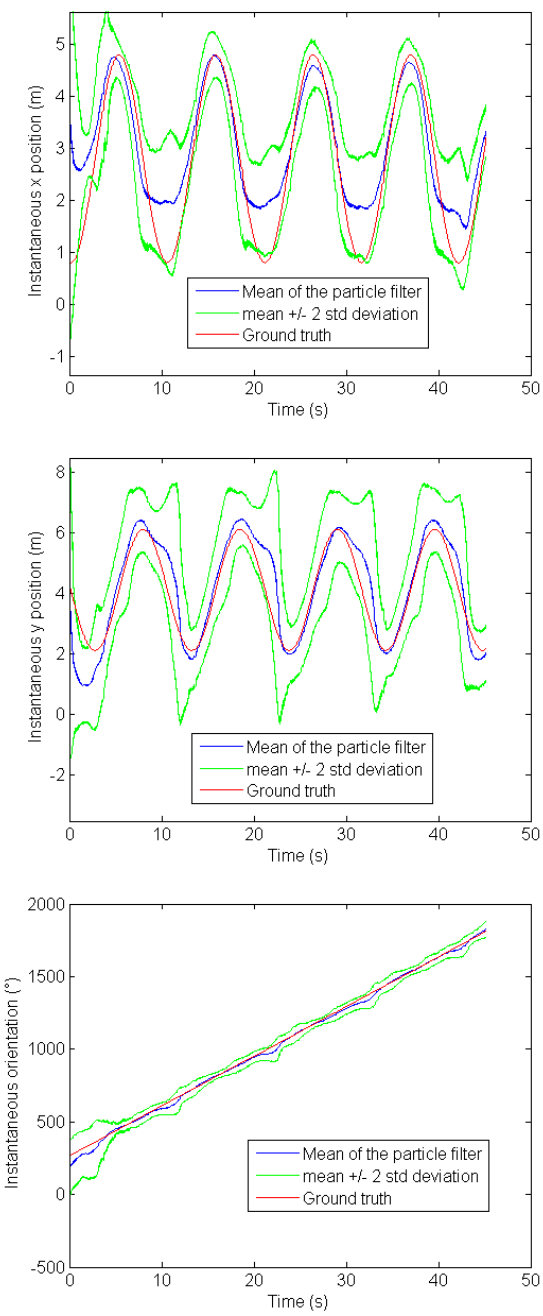

Fig. 7. Comparison of the mean instantaneous position (top: x, middle: y) and orientation (bottom) of the particle filter with the ground truth in the case of the circle trajectory.

The gain in precision compared to typical results obtained for a localization using Wi-Fi information is considerable. In those applications, the reported positioning errors are on the order of a few meters ([7], [8], [9], and [10]). For the straight line trajectory (Fig. 6), after a few seconds, the mean of the particle cloud is always within 0.7m of the ground truth position and within 25° of the ground truth orientation.

In the case of the circle trajectory (Fig. 7), the mean position of the particle filter is also close to the ground truth when it is not bimodal. The periodic big difference between the ground truth and the particle filter's mean is due to bimodality. Particles which entered the right mode survive and the other ones are eliminated in the next few seconds. The graphs above are the result of instantaneously estimating the position by taking the mean of the particle filter. If better accuracy is desired and if it is acceptable to wait a few seconds, it is preferable to estimate the position a

posteriori by only averaging the past positions of particles which survived [5]. This would lead to a better position estimation, especially where the instantaneous estimate was poor because of multi-modal distributions.

The quality of the localization reflects the rich information contained in the three components of the magnetic field and its high signal to noise ratio. The vertical component and the magnitude of the horizontal component provide information about the position whereas the angle of the horizontal component gives information about the orientation.

VII. Conclusion

We presented a real time indoor localization method that utilizes a single 3-axis magnetometer to estimate the location of a handheld device. Using an online particle filter, we achieved localization accuracy of 0.7 meters in position and 25 degrees in orientation for the simple straight line trajectory. The localization of the circle trajectory gave a slightly higher instantaneous position error (up to 1.2m) and orientation error (up to 40°). Those results must be interpreted with care because better results would easily be obtained by using an a posteriori position estimate. They demonstrate that indoor localization based solely on magnetometer and accelerometer data is possible.

The main limitation of this indoor localization approach is the necessity of creating magnetic field maps. Therefore, we presented a fast 2D mapping technique and demonstrated it in a square room. Generalization of the technique to non-square rooms with obstacles (Fig. 8) is possible by replacing the lines X_i and Y_j by a list of segments. The energy minimization algorithm can then be modified by replacing the constraints on the lines' intersections by constraints on the segments' intersections.

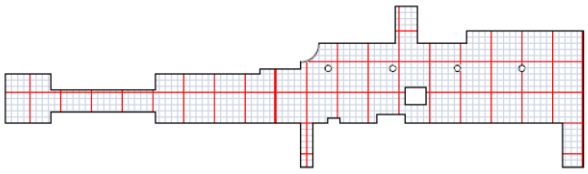

Fig.8. Example of mapping strategy for a more complex environment. Physical map of the Packard Atrium at Stanford University. The grid inside the contour represents the segments to follow in order to build the magnetic field map.

Magnetometers are part of all smartphones but are still under-used. Wi-Fi antennas are perfect to locate a phone user on the globe up to the building or room level. Gyroscopes and accelerometers provide movement information. We showed that magnetometers can complement the previous sensors by determining the phone user's position and orientation inside the room. To emphasis the value of magnetometers, this work focused on using only a magnetometer and an accelerometer for localization. Because they lack global positioning capability, it is as a complement to existing localization systems that the magnetometers have the more potential, possibly transforming five-meter accurate Wi-Fi- or GPS-based systems into one-meter, 20-degree accurate techniques.

Acknowledgment

The authors would like to acknowledge the following individuals from Stanford University:

- David Stavens, Alex Teichman and Jesse Levinson for providing feedback and project guidance.

- Nicole Rodia and Anand Atreya, Joseph Huang, David Millman and Ricky Roesler for the constructive discussions and shared insights on phone-based and Wi-Fi localization.

- Morgan Quigley for providing the data logging framework for the phone.

References

[1] D. Roetenberg, H. Luinge and P. Veltink. "Inertial and magnetic sensing of human movement near ferromagnetic materials", *ISMAR* 2003

[2] J. Haverinen, A. Kemppainen, "Global indoor self-localization based on the ambient magnetic field", *Robotics and Autonomous Systems 57* (2009) 1028-1035.

[3] S. Suksakulchai, S. Thongchai, D. M. Wilkes, and K. Kawamura. "Mobile Robot Localization using an Electronic Compass for Corridor Environment", *Proceedings of the IEEE International Conference on Systems, Man, and Cybernetics*, 2000.

[4] D. Vissière, A. Martin, N. Petit, "Using magnetic disturbances to improve IMU-based position estimation", *Proceedings of the European Control Conference*, 2007

[5] D. Gebre-Egziabher, G. H. Elkaimy, J. D. Powell, and B. W. Parkinson, "A non-linear, two-step estimation algorithm for calibrating solid-state strapdown magnetometers", *Proceedings of the Eighth International Conference on Integrated Navigation Systems*, 2001

[6] S. Thrun, W. Burgard, and D. Fox. *Probabilistic Robotics*. Cambridge, MA: MIT Press, 2005.

[7] G. Retscher E. Moser, D. Vredeveld, D. Heberling, and J. Pamp, "Performance and accuracy test of a WiFi indoor positioning system", *Journal of Applied Geodesy*, 2007.

[8] J. Rantakokko, J. Rydell, P. Stromback, P. Handel, J. Callmer, D. Tornqvist, F. Gustafsson, M. Jobs, M. Gruden, "Accurate and reliable soldier and first responder indoor positioning: multisensor systems and cooperative localization", *Wireless Communications, IEEE*, 2011

[9] J. Biswas, M. Veloso, "Wifi localization and navigation for autonomous indoor mobile robots", *Proceedings of the IEEE International Conference on Robotics and Automation*, 2010

[10] E Martin, O Vinyals, G Friedland, R. Bajcsy, "Precise indoor localization using smart phones", *Proceedings of the international conference on Multimedia*, 2010